Analysis of Reaction-Transport Phenomena in a Microfluidic System for the Detection of IgG*

M. PŘIBYL**, V. KNÁPKOVÁ, D. ŠNITA, and M. MAREK

Department of Chemical Engineering and Center for Nonlinear Dynamics of Chemical and Biological Systems, Institute of Chemical Technology, CZ-166 28 Prague
e-mail: Michal.Pribyl@vscht.cz

Received 1 April 2005

A spatially two-dimensional mathematical model of microfluidic biosensor for immunological determination of human immunoglobulin G (IgG) with the use of Protein A (PA) immobilized on the internal walls of a microchannel is presented. Convection flow in the microdevice is induced by an imposed difference of electric potential (electroosmosis). In the model, the electroosmotic convection is described using the slip boundary conditions that can be defined by the Helmholtz—Smoluchowski equation.

Incubation phase (formation of the immobile PA—IgG complex) of the immunoassay has been studied. Effects of the antibody concentration in a sample, the imposed difference of electric potential, the surface heterogeneities in the reaction zone, and other model parameters on the saturation time were determined.

It was found that the surface heterogeneities could form complex velocity fields at the location of the adsorption zone: either an intensive flow at the microchannel walls or the nozzle-like flow. Generally, the local acceleration of the flow causes the decrease of the mass-transfer resistance. Further, imposed electric field of a proper orientation was able to shorten the incubation phase to 600 s, assuming the microchannel device with the diameter of 100 μm and the chosen reaction kinetics. Hence, the incubation phase could be substantially reduced enabling, *e.g.*, fast diagnostics.

Simulation of the effects of the antibody sample concentration revealed good qualitative agreement with experimental data obtained in a similar microfluidic device (published by *Dodge et al.*, *Anal. Chem. 73*, 3400 (2001)).

The last decade brought many interesting applications of microtechnology in the area of chemical, biochemical, and biological systems. One of the most studied problems is the detection, amplification, and sequencing of DNA or RNA strands. For example, *Mitnik et al.* [1] reviewed the use of capillary electrophoresis in microchips for DNA sequencing that can substantially accelerate the genome analysis. Recently, *Slater et al.* [2] described new possibilities of fast and efficient DNA strand separation in microfluidic devices. *El-Ali et al.* [3] developed PCR microchip on the polymer SU-8 platform for fast amplification of DNAs. The PCR procedure requires fast and controllable temperature changes that can be in microchips provided due to extremely high value of the internal surface to volume ratio. Currently, numerous research groups investigate microarrays and microfluidic chips for protein screening (*e.g.* the screening of antibodies). *Glökler* and *Angenendt* [4] recently reviewed the progress in the development of microfluidic platform for the protein detection in diagnostics, proteomics, and therapeutics. Main reason for the use of microdevices for biochemical applications is the high cost of pure reagents (*e.g.* antigens and antibodies) and substantially reduced time of the assays (mostly in diagnostics and genomics) [5, 6].

Heterogeneous immunoassay in microstructures is also intensively studied. Recently, *Yakovleva et al.* [7] reported an investigation of immunosensors with immobilized proteins A and G for the detection of immunoglobulins G. The microchip design enables regeneration of the antigen-binding sites and repeated use of the microchip for the period of 8 months. *Wang* [8] discussed possible use of immunomicrofluidic platforms for the detection of weapons of mass destruction. *Lin et al.* [9] and *Song* and *Vo-Dinh* [10] developed heterogeneous microchip systems for immunological detection of *Helicobacter Pylori* and *Escherichia*

*Presented at the 32nd International Conference of the Slovak Society of Chemical Engineering, Tatranské Matliare, 23—27 May 2005.

**The author to whom the correspondence should be addressed.

coli, respectively. *Lin et al.* [9] found that the required volumes of expensive reactants were 100-fold less than those of conventional immunoassay systems. *Song* and *Vo-Dinh* [10] also stressed the advantages of their platform: low cost, compactness, possible reuse, and regeneration.

The electrokinetic transport (electrophoresis and/or electroosmosis) is often used in microchips instead of the classical pressure-driven flow [11—15]. When an electric charge is bound on the microchannel walls, an imposed electric field can induce convective flow of an electrolyte in the microstructure. However, the electroosmotic mobility strongly depends on properties of the microchannel material and the electrolyte composition [16], *e.g.* the electroosmotic convection locally varies when macromolecules bind to the surface. Then, changes in the electric charge distribution could be observed [17].

As the fluid control is a crucial element of the microfluidic devices, a number of models of the electrokinetic flow have been proposed [18]. *Dutta* and *Beskok* [19] found that the slip boundary approach (based on the Helmholtz—Smoluchowski equation) brings only a several percent error in the solution of Navier—Stokes and continuity equations. However, description of the processes in a microchannel is substantially simplified as the effects in the electric double layer could be neglected. Numerical calculations of the electroosmotic flow on the T microchannel geometry were reported in [20, 21] and on the cross-shape geometry in [22, 23].

In this work, a mathematical model of the spatially two-dimensional microchip with complex geometry for heterogeneous immunoassay was developed. The model equations describe the distribution of velocity, pressure, electric potential, and concentrations of a soluble antibody and bounded antigen—antibody complex in the proposed microchip. As a model biochemical system protein A (PA)—immunoglobulin G (IgG) assay was considered. PA specifically binds to IgG, which is widely used to detect immunoglobulins. Corresponding kinetic and transport data were taken from [17].

Main goal of this study was to develop a multiphysics mathematical model that would be useful for the prediction and verification of physical and chemical processes inside a complex microchannel structure with different characteristic dimensions (*e.g.* microchannel diameter and length) and for a fast biosensor design. A number of papers have already dealt either with the problems of convective and/or electrokinetic transport in microfluidic devices or with the experiments focused on immunoassays in such devices. Presented model combines both these areas with the use of physical and chemical description of the processes inside the microstructure and experiences reported in the experimental immunoassays [7, 17].

A systematic study of the effects of transport, kinetics, and other parameters on the dynamics of the heterogeneous PA—IgG immunoassay was carried out to determine model parameters, for which a short incubation period could be obtained. Moreover, qualitative comparison of received results with the reported experimental data is presented.

THEORETICAL

Microchip comprising four arms for the introduction or removal of antibody samples, buffers, and regenerative solutions and one central channel was considered (Fig. 1). There was an active layer of the immobilized antigen situated in the middle of the central channel. When the solution of sample containing the antibody (IgG) was brought into the contact with the layer of immobilized antigen (PA), formation of the antigen—antibody complex started. Direction of the convection flow of solution was controlled electrokinetically by an external electric field imposed on the chosen reservoirs (Fig. 1).

Potentially, microsystems can be integrated into microanalytical systems using heterogeneous immunoassay. The zone of the immobilized antigen or antibody is defined as the zone of the detection. The side channels serve for the introduction of chemical/biochemical components to the reaction/detection zone. Typical immunoassay protocol consists of several steps, *e.g.* washing, introduction of a primary antibody and antigen—antibody complex formation, washing, introduction of a secondary antibody and incubation, washing and detection. Each component of the immunoassay (buffers and antibodies) is placed in

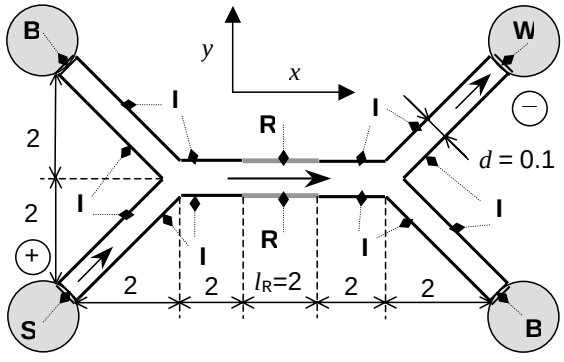

Fig. 1. The scheme of the microchip for heterogeneous immunoassay. The width of all channels is $d = 100$ μm and the length of the reaction zone with the antigen-binding sites $l_R = 2$ mm. Dimensions of the other parts of the microchip are shown in millimeters. The arrow indicates the direction of the convection flow in the incubation phase. The symbols S, W, B, R, and I denote the sample reservoir, the waste reservoir, the buffer reservoir, the walls of the microchannels with the immobilized antigen, and the inert walls (without the antigen), respectively. The orthogonal x—y system is considered as coordination system.

a special reservoir that is connected with the reaction zone by a special arm. The detection can be carried out, *e.g.* by means of fluorescence or surface plasmon resonance methods.

During the incubation period, *i.e.* formation of immobile PA—IgG complex, fully developed field of flow, pressure, and electric potential was assumed. Small variations of the antibody concentration in different parts of the microstructure should not affect the velocity field significantly. Then, the equation of the momentum conservation and the continuity equation could be written in the following form

$$\rho \boldsymbol{v} \cdot \nabla \boldsymbol{v} = -\nabla p + \mu \nabla^2 \boldsymbol{v} \qquad \nabla \cdot \boldsymbol{v} = 0 \tag{1}$$

where ρ represents liquid density, μ is dynamic viscosity of the liquid, $\boldsymbol{v}$ is velocity vector and ∇p is the pressure gradient.

Instead of the electric body force, the slip boundary conditions on the microchannel walls, *i.e.* the nonzero velocity on these boundaries was considered. The slip boundary conditions are defined by the Helmholtz—Smoluchowski equation [16]

$$\boldsymbol{v} = -\frac{\varepsilon \zeta}{\mu} \nabla \Phi \approx -\mu_{\mathrm{eo}} \nabla \Phi \tag{2}$$

where ε is the environment permittivity, μ is the dynamic viscosity of an electrolyte, ζ is the zeta potential, $\nabla \Phi$ is the local gradient of electric potential, and μ_{eo} is the electroosmotic mobility coefficient.

Then, the velocity and the pressure boundary condition can be written as

$$\boldsymbol{v}\,|_{\mathrm{I,S}} = -\mu_{\mathrm{eo}} \nabla \Phi\,|_{\mathrm{I,S}} \qquad \boldsymbol{v}\,|_{\mathrm{R}} = -\mu_{\mathrm{eor}} \nabla \Phi\,|_{\mathrm{R}}$$

$$\boldsymbol{v}\,|_{\mathrm{B}} = 0 \qquad p|_{\mathrm{W}} = 0 \tag{3}$$

Indices used in the boundary conditions correspond to the notation of Fig. 1.

As the electric conductivity is approximately constant in the entire microstructure (it is given by the carrier electrolyte of the sample; the antibody contribution to the overall conductivity is negligible), distribution of the electric potential is given by the solution of the Laplacian

$$\nabla \cdot \nabla \Phi = 0 \tag{4}$$

Electroosmotic transport is induced by the potential difference $\Delta \Phi$ between the sample (S) and the waste (W) compartments and the other boundaries (B, I, R) are considered to be electric insulators

$$\Delta \Phi = \Phi\,|_{\mathrm{S}} - \Phi\,|_{\mathrm{W}} \quad \boldsymbol{n} \cdot \nabla \Phi\,|_{\mathrm{I,R,B}} = 0 \tag{5}$$

where $\boldsymbol{n}$ is the normal vector.

The distribution of IgG can be evaluated from the mass balance, where the total flux of the antibody $\boldsymbol{J}_{\mathrm{Ab}}$ is given by the sum of convection, diffusion, and electromigration fluxes

$$\frac{\partial c_{\mathrm{Ab}}}{\partial \tau} = -\nabla \cdot \boldsymbol{J}_{\mathrm{Ab}}$$

$$\boldsymbol{J}_{\mathrm{Ab}} = \boldsymbol{v} c_{\mathrm{Ab}} - D_{\mathrm{Ab}} \nabla c_{\mathrm{Ab}} - \frac{z_{\mathrm{Ab}} D_{\mathrm{Ab}} F}{R_T T} c_{\mathrm{Ab}} \nabla \Phi \tag{6}$$

where symbols c_{Ab}, τ, D_{Ab}, z_{Ab}, F, R_T, and T represent antibody concentration, time, antibody diffusivity, antibody charge number, Faraday's constant, molar gas constant, and temperature, respectively.

Dirichlet boundary conditions on the inlets and the outlets of the system, *i.e.* a constant composition of the electrolytes, were assumed. Zero IgG flux was considered on the internal walls except the reaction zone, where the IgG—PA complex (C) was formed according to the scheme

$$\mathrm{IgG} + \mathrm{PA} \underset{}{\overset{k_{\mathrm{c}}}{\rightleftharpoons}} \mathrm{C} \tag{A}$$

Then, the boundary conditions could be written as

$$c_{\mathrm{Ab}}\,|_{\mathrm{S}} = c_{\mathrm{Ab,S}} \quad c_{\mathrm{Ab}}\,|_{\mathrm{W,B}} = 0$$

$$\boldsymbol{n} \cdot \boldsymbol{J}_{\mathrm{Ab}}\,|_{\mathrm{I}} = 0 \quad \boldsymbol{n} \cdot \boldsymbol{J}_{\mathrm{Ab}}\,|_{\mathrm{R}} = -r_{\mathrm{c}} \tag{7}$$

where the rate of the complex formation, r_{c}, is defined as

$$r_{\mathrm{c}} = -k_{\mathrm{c}} \left[K_{\mathrm{d}} c_{\mathrm{c}} - c_{\mathrm{Ab}}\,|_{\mathrm{R}} \left(c_{\mathrm{Ag,tot}} - c_{\mathrm{c}} \right) \right] \tag{8}$$

where the symbols k_{c}, K_{d}, and $c_{\mathrm{Ag,tot}}$ denote the kinetic constant of IgG—PA complex formation, the equilibrium dissociation constant of the IgG—PA complex, and the total surface concentration of PA, respectively. Eqn (*8*) arises if the equation for dissociation equilibrium of the IgG—PA complex $K_{\mathrm{d}} = k_{\mathrm{d}}/k_{\mathrm{c}}$ and the relationship for the total surface concentration of the immobilized antigen $c_{\mathrm{Ag,tot}} = c_{\mathrm{Ag}} + c_{\mathrm{c}}$ are substituted into the basic kinetic equation of the complex formation $r_{\mathrm{c}} = k_{\mathrm{c}} c_{\mathrm{Ab}} c_{\mathrm{Ag}} - k_{\mathrm{d}} c_{\mathrm{c}}$. Here, c_{Ag} represents the surface concentration of the free antigen and k_{d} is the kinetic constant of the IgG—PA complex dissociation.

The surface concentration of the IgG—PA complex is then given by

$$\frac{\partial c_{\mathrm{c}}}{\partial \tau} = r_{\mathrm{c}} \tag{9}$$

The microchip free of the antibody and the antigen—antibody complex is considered as an initial condition for the dynamic simulations. The parameter values used in simulations are summarized in Table 1 and in the figure captions.

Eqns (*1*), (*4*), (*6*), and (*9*) together with the boundary conditions (*3*), (*5*), and (*7*) form the mathematical model of the incubation phase of the immunoassay in the microchip. Both steady-state and

Table 1. Model Parameters

Parameter	Value
Diameter of the microchannels, d/m	1×10^{-4}
Dimension of the zone with the immobilized antigen, l_R/m	2×10^{-3}
Faraday's constant, F/(C kmol^{-1})	9.6487×10^{7}
Antibody—antigen complex dissociation constant, K_d/(kmol m^{-3})	2.53×10^{-3}
Molar gas constant, R_T/(J kmol^{-1} K^{-1})	8.314×10^{3}
Temperature, T/K	310
Antibody charge number, z_{Ab}	0
Electrolyte viscosity, μ/(Pa s)	6.92×10^{-4}
Electroosmotic mobility at the inert microchannel walls, μ_{eo}/(m^2 V^{-1} s^{-1})	1×10^{-8}
Electrolyte density, ρ/(kg m^{-3})	1×10^{3}

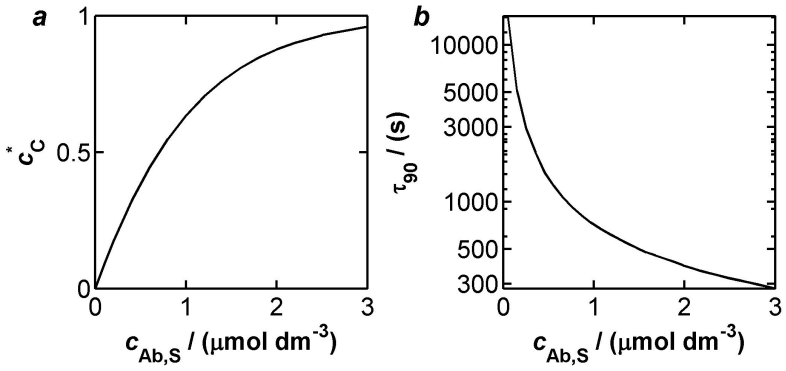

Fig. 2. Effects of antibody concentration in the sample. *a*) Dependence of the normalized PA—IgG complex concentration on the antibody concentration in the sample at time 360 s. *b*) Dependence of the saturation time on the antibody concentration in the sample. Other parameter values are $\Delta\Phi = 100$ V, $\mu_{eor} = 1 \times 10^{-8}$ m^2 V^{-1} s^{-1}, $D_{Ab} = 4 \times 10^{-11}$ m^2 s^{-1}, $k_c = 3.952 \times 10^{3}$ m^3 kmol^{-1} s^{-1}, $c_{Ag,tot} = 1 \times 10^{-10}$ kmol m^{-2}.

nonstationary analysis have been carried out by means of the standard Matlab/Femlab solver based on the finite element method. Using this software, the steady-state distribution of velocity, pressure, and electric potential for the chosen set of parameters was computed. The results of the steady-state analysis together with the concentrations of IgG and IgG—PA complex, which were set to zero, were used as the initial condition for the dynamic simulation of the antigen—antibody complex formation.

Auxiliary variables were defined in order to quantify the parametric studies. Spatially averaged and normalized dimensionless complex concentration was defined as

$$c_c^* \equiv (1/l_R) \int_R (c_c/c_{Ag,tot}) dx \qquad (10)$$

where l_R is the length of the reaction zone and τ_{90} is the saturation time, at which the average PA—IgG complex concentration reaches 90 % of the total concentration of the immobilized antigen ($c_c^* = 0.9$). The dimensionless concentration c_c^* can be simply connected to the experimentally observed quantities. For example, the intensity of a fluorescence signal from the reaction/detection zone is proportional to the total amount of the formed antigen—antibody complex. The surface complex concentration or the total number of the formed complex molecules can be directly computed from knowledge of c_c^* and the surface concentration of the immobilized antigen.

RESULTS AND DISCUSSION

The incubation phase of the immunoassay was carried out in a specified time period that was the same in all experiments in order to quantify the amount of the antibody in the sample solution. *Dodge et al.* [17] studied the dependence of the intensity of the fluorescence signal on the antibody concentration in the sample after the incubation period lasting 200 s. In this study, very similar behaviour was observed for the incubation period equal to 360 s (Fig. 2*a*). As intensity of the expected signal is proportional to the spatially averaged IgG—PA complex concentration, the curve presented in Fig. 2*a* represents a typical calibration curve for the quantitative immunoassay.

The dependence of the saturation time on the antibody concentration in the sample is shown in Fig. 2*b*. Saturation time decreases with the growing concentration of the antibody in the sample as the system shifts from the transport-limited to the reaction-limited regime. Parametrical study presented in Fig. 2 reveals that the incubation phase of the immunoassay will not exceed several hundreds of seconds for the proposed arrangement and for typical parameters of the PA—IgG interaction.

At given conditions, the growing electric field intensity accelerates electroosmotic transport of particles and therefore also the complex formation. The dependence of the normalized PA—IgG concentration on the imposed electric potential difference at a time

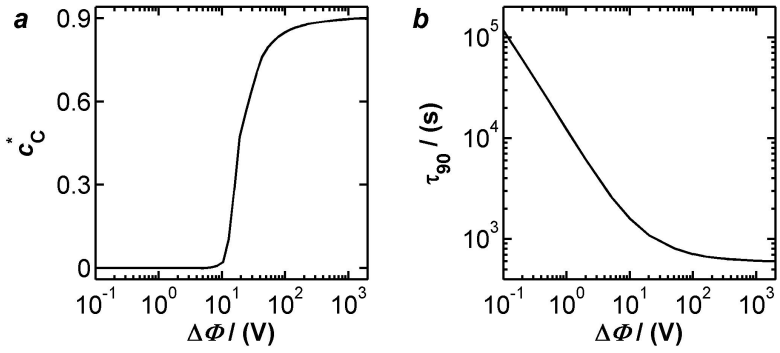

Fig. 3. Effects of magnitude of the imposed electric field. *a*) Dependence of the normalized antibody—antigen complex concentration on the imposed difference of electric potential at time 600 s. *b*) Dependence of the saturation time on the imposed difference of electric potential. $c_{\mathrm{Ab,S}} = 1\ \mu$M and other parameters are the same as in Fig. 2.

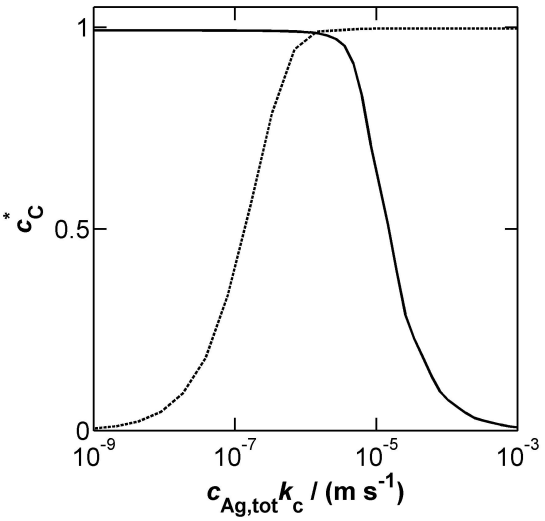

Fig. 4. Dependence of the spatially averaged complex concentration on the product of the total concentration of the immobilized antigen and the antigen-antibody binding constant 600 s after the start of the incubation. $c_{\mathrm{Ag,tot}} = 1 \times 10^{-10}$ kmol m^{-2} (dotted line), $k_{\mathrm{c}} = 1 \times 10^4$ m^3 kmol^{-1} s^{-1} (solid line). $c_{\mathrm{Ab,S}} = 1\ \mu$M and other parameters are the same as in Fig. 2.

of 600 s is plotted in Fig. 3*a*. For $\Delta\Phi/\mathrm{V} < 10^1$, the convective transport of the antibody molecules from the sample reservoir is too slow to reach the antigen-binding sites within the chosen time interval of 600 s. On the other hand, for the potential difference $\Delta\Phi/\mathrm{V} > 10^2$, the reaction equilibrium is nearly reached during the chosen time period. That means that the choice of the electric potential difference may drastically affect the time course of the immunoassay and the result of a prospective experiment.

Dependence of the saturation time on the applied potential difference is shown in Fig. 3*b*. For lower potential differences $\Delta\Phi/\mathrm{V} \in \langle 10^{-1}, 10^1 \rangle$, the saturation time decreases (numerical value of the slope is ≈ -1 in the logarithmic plot) with the increase of the electric potential difference. For larger differences of electric potential the curve asymptotically approaches a finite rate of the PA—IgG complex formation (≈ 600 s).

Influence of both, concentration of the immobilized antigen and the rate constant of the antigen—antibody complex formation on the attainability of the saturation level of the antigen-binding sites is opposite each other (Fig. 4). The growing concentration of the antigen caused a decrease of the saturation level within a selected time of the immunoassay as the number of free binding sites was increased. Conversely, when the value of kinetic constant of the complex formation was increased, the saturation level increased as the immobilized antigen firmly bonded to the antibody molecules. Both, antigen concentration and rate constant of the antigen—antibody complex formation may be varied within an order of several magnitudes during an immunoassay. Hence, a suitable concentration of immobilized antigen has to be considered for a particular immunoassay in order to avoid an increase of the time requirements of the incubation phase.

Electroosmotic mobility depends both on the electrolyte properties and the character of the internal surface of the microchannels. The antigen immobilization in the reaction zone can locally modify the ζ-potential and thus the value of electroosmotic mobility coefficient.

First, the steady-state distribution of velocity and pressure in the microdevice for selected values of electroosmotic mobility in the reaction zone was evaluated. The detail of the received velocity streamlines between two plates that form the reaction zone is plotted in Fig. 5. Then, the evolution of distribution of antibody concentration in the microchip was computed. Details of antibody concentration distributions between the two plates with the immobilized antigen for different values of the electroosmotic mobility coefficient calculated at the time of 80 s from the sample solution introduction into the microchip are plotted in Fig. 6. The antibody distributions are not axially symmetric because the inlet of the sample from the S microchannel to the central channel breaks spatial symmetry of numerical solution (Fig. 1).

After the protein immobilization, density of the bound negative charge could be higher in the reaction zone than on the remaining microchip walls. Therefore, the velocity close to the microchannel walls would be higher in the reaction zone. Consequently, the backflow of the electrolyte would be observed in the centre of the microchannel (Fig. 5*a*). Thus, the antibody

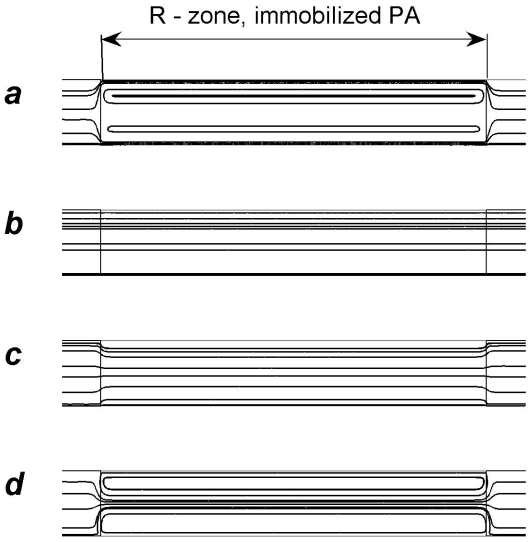

Fig. 5. Velocity streamlines at the location of the immobilized antigen in the steady state. *a*) $\mu_{\mathrm{eor}} = 1 \times 10^{-7}$ m^2 V^{-1} s^{-1}, *b*) $\mu_{\mathrm{eor}} = 1 \times 10^{-8}$ m^2 V^{-1} s^{-1}, *c*) $\mu_{\mathrm{eor}} = 0$ m^2 V^{-1} s^{-1}, *d*) $\mu_{\mathrm{eor}} = -1 \times 10^{-7}$ m^2 V^{-1} s^{-1}. $\Delta\Phi = 100$ V.

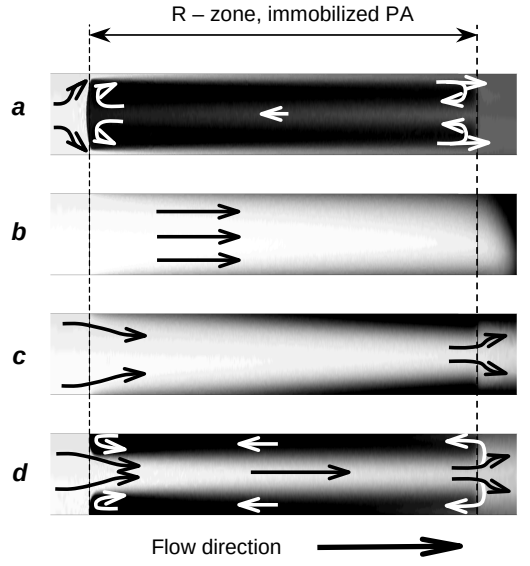

Fig. 6. Distribution of antibody concentration at the location of the immobilized antigen at time 80 s after the introduction of the sample solution. *a*) $\mu_{\mathrm{eor}} = 1 \times 10^{-7}$ m^2 V^{-1} s^{-1}, *b*) $\mu_{\mathrm{eor}} = 1 \times 10^{-8}$ m^2 V^{-1} s^{-1}, *c*) $\mu_{\mathrm{eor}} = 0$ m^2 V^{-1} s^{-1}, *d*) $\mu_{\mathrm{eor}} = -2 \times 10^{-8}$ m^2 V^{-1} s^{-1}. Other parameters are $c_{\mathrm{Ab,S}} = 1$ μM, $\Delta\Phi = 100$ V, $D_{\mathrm{Ab}} = 1 \times 10^{-11}$ m^2 s^{-1}, $k_{\mathrm{c}} = 3.952 \times 10^3$ m^3 kmol^{-1} s^{-1}, $c_{\mathrm{Ag,tot}} = 1 \times 10^{-10}$ kmol m^{-2}. White areas depict regions with a high antibody concentration. Black areas mean the space free of antibody. The arrows show flow direction in a part of the microchannel.

particles principally approach the walls with immobilized antigen, *i.e.* the binding sites for the antigen—antibody complex formation (Fig. 6*a*).

The velocity and the IgG concentration fields for the homogeneous distribution of negative charge in the entire microstructure ($\mu_{\mathrm{eo}} = \mu_{\mathrm{eor}}$) are plotted in Figs. 5*b*, 6*b*.

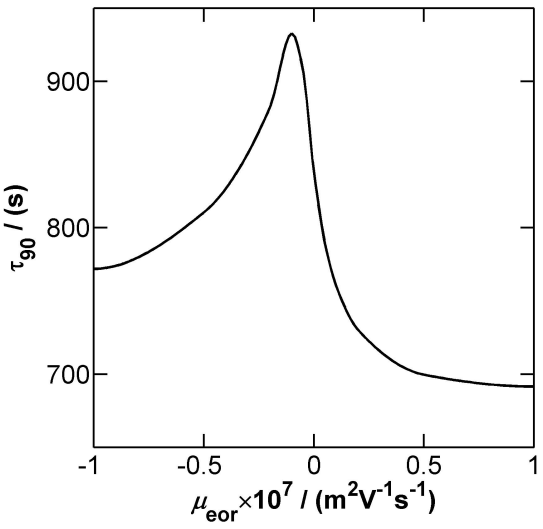

Fig. 7. Dependence of the saturation time on the electroosmotic mobility coefficient in the reaction zone. Other parameters are the same as in Fig. 6.

Due to the immobilization of macromolecules on the microchannel walls, the density of the bound negative charge can decrease. Figs. 5*c* and 6*c* present computed distribution of the velocity and the IgG concentration for the electroosmotic coefficient equal to zero at the location of the immobilized antigen. The velocity profile corresponded to a typical parabolic shape for the pressure-driven convection with zero velocity on the walls of the reaction zone. Intensity of the antibody molecules transport to the microchannel walls decreased as it was driven by the diffusion only.

If a chemical modification or the immobilization of the antigen in the reaction zone results in the accumulation of the positive charge on the channel walls, the reaction zone works like a nozzle. The backflow at the channel walls causes an increase of the convection velocity in the centre of the channel (Fig. 5*d*). Hence, the antibody molecules do not reach the microchannel walls with immobilized antigen situated closer to the sample inlet. However, the backflow at the channel walls returns the antibody molecules back to the antigen-binding sites (Fig. 6*d*).

The dependence of the saturation time on the electroosmotic mobility coefficient has a nonmonotonous character (Fig. 7). The shortest time to saturate negatively charged active zone was necessary when the density of the bound negative charge was high (*e.g.* $\mu_{\mathrm{eor}} = 1 \times 10^{-7}$ m^2 V^{-1} s^{-1}) due to the fast convection flow near the channel walls. The maximum saturation time was observed for $\mu_{\mathrm{eor}} = -1 \times 10^{-8}$ m^2 V^{-1} s^{-1}. However, when the electroosmotic mobility coefficient was further decreased (*e.g.* $\mu_{\mathrm{eor}} = -1 \times 10^{-7}$ m^2 V^{-1} s^{-1}), saturation time was reduced again. This effect is

caused by the intense backflow that returns free antibody molecules directly to the microchannel walls where the PA-binding sites are quickly occupied.

The developed mathematical model can be used for numerical analysis of geometrically different systems frequently occurring in microfluidics. There is a limitation of the model if the diameter of the microchannel is less than several microns. Then the processes close to the electrically charged channel walls cannot be neglected and the Helmholtz—Smoluchowski approximation used in this model is unacceptable. Most of the heterogeneous immunoassays are carried out at similar conditions – pH, buffer concentration, temperature, *etc.* However, there are large variations in the surface concentrations of proteins and in the values of kinetic and equilibrium parameters. Effects of these parameters can be simply studied by means of this model. Hence, the mathematical model can be used for large parametrical studies of particular immunoassay systems. Geometrical, kinetic, concentration, and transport parameters can be tested. Arrangements suitable for experimental studies can be then selected.

Acknowledgements. The authors thank for the support of the research by the Grant 104/03/D006 of the Czech Grant Agency.

REFERENCES

1. Mitnik, L., Novotný, M., Felten, C., Buonocore, S., Koutný, L., and Schmalzing, D., *Electrophoresis 22*, 4104 (2001).
2. Slater, G. W., Guillouzic, S., Gauthier, M. G., Mercier, J. F., Kenward, M., McCormic, L. C., and Tessier, F., *Electrophoresis 23*, 3791 (2002).
3. El-Ali, J., Perch-Nielsen, I. R., Poulsen, C. R., Bang, D. D., Telleman, P., and Wolff, A., *Sens. Actuators, A 110*, 3 (2004).
4. Glökler, J. and Angenendt, P., *J. Chromatogr., B 797*, 229 (2003).
5. Heller, M. J. and Guttman, A., *Integrated Microfibrated Biodevices.* Dekker, New York, 2002.
6. Přibyl, M., Šnita, D., Hasal, P., and Marek, M., *Chem. Eng. J. 101*, 303 (2004).
7. Yakovleva, J., Davidsson, R., Bengtsson, M., Laurell, T., and Emnéus, J., *Biosens. Bioelectron. 19*, 21 (2003).
8. Wang, J., *Anal. Chim. Acta 507*, 3 (2004).
9. Lin, F. Y. H., Sabri, M., Erickson, D., Alirezaie, J., Li, D., and Sherman, P. M., *Analyst 129*, 823 (2004).
10. Song, J. M. and Vo-Dinh, T., *Anal. Chim. Acta 507*, 115 (2004).
11. Guijt, R. M., Baltussen, E., and van Dedem, G. W. K., *Electrophoresis 23*, 823 (2002).
12. Rossier, J., Reymond, F., and Michel, P. E., *Electrophoresis 23*, 858 (2002).
13. Schmalzing, D., Buonocore, S., and Piggee, C., *Electrophoresis 21*, 3919 (2000).
14. Tmej, F., Hasal, P., Limbergová, Z., Chmelíková, R., and Marek, M., *Chem. Pap. 55*, 339 (2001).
15. Yeung, W. S. B., Luo, G. A., Wang, Q. G., and Ou, J. P., *J. Chromatogr., B 797*, 217 (2003).
16. Probstein, R. F., *Physicochemical Hydrodynamics: An Introduction.* Wiley and Sons, New York, 1994.
17. Dodge, A., Fluri, K., Verpoorte, E., and de Rooij, N. F., *Anal. Chem. 73*, 3400 (2001).
18. Li, D., *Colloids Surf., A 195*, 35 (2001).
19. Dutta, P. and Beskok, A., *Anal. Chem. 73*, 1979 (2001).
20. Bianchi, F., Ferrigno, R., and Giraut, H. H., *Anal. Chem. 72*, 1987 (2000).
21. MacInnes, J. M., *Chem. Eng. Sci. 57*, 4539 (2002).
22. Ermakov, J., Jacobson, S. C., and Ramsey, J. M., *Anal. Chem. 72*, 3512 (2000).
23. Jin, Y. and Luo, G. A., *Electrophoresis 24*, 1242 (2003).